Pore-scale network model for three-phase flow in mixed-wet porous media

M. I. J. van Dijke* and K. S. Sorbie
Institute of Petroleum Engineering, Heriot-Watt University, Riccarton, Edinburgh EH14 4AS, Scotland, United Kingdom
(Received 12 October 2001; revised manuscript received 18 July 2002; published 2 October 2002)

We describe the development and application of a three-dimensional pore-scale network simulator for modeling capillary-dominated three-phase flow in porous media where the wettability varies from pore to pore, i.e., where each pore is allowed to have a different oil-water contact angle from a chosen distribution. Physical constraint equations for the remaining gas-oil and gas-water contact angles are implemented. In weakly wetted pores wetting films are absent, which reduces the continuity of the various phases in the network and increases the number of phase clusters that are disconnected from inlet or outlet. Mobilization of disconnected clusters requires incorporation of double and *multiple* displacement chains that involve a string of neighboring phase clusters, e.g., gas→oil→gas→oil→water. Furthermore, when multiple displacement chains cause disconnected clusters to reconnect to the outlet, the phase pressures at the outlet boundary are updated consistent with the pressures within the system. A number of benchmark simulations for systems with nonuniform wettability, mixed-wet with the larger pores oil-wet, are presented. The outcome of these simulations is presented as phase paths in saturation space and in the form of pore occupancy histograms and histograms of the length and type of displacement chains. Comparison of simulated saturation paths with those of an analytical capillary bundle model with the same wettability show good agreement where phase continuity is high and decreasing agreement as phase continuity in the network decreases. The saturation paths and occupancy and displacement statistics for a number of water-alternating-gas injection (WAG) simulations bring out the various features of the model, in particular, those related to the wettability. We find that multiple displacements do occur, mainly during higher-order WAG floods, although their effect on oil recovery seems limited. Variation of the outlet boundary pressure differences has an effect in certain regions of the saturation space that are defined by the analytical model.

DOI: 10.1103/PhysRevE.66.046302 PACS number(s): 47.55.Mh, 68.08.Bc

I. INTRODUCTION

Three-phase flow in porous media is important in areas such as aquifer remediation from nonaqueous phase liquids (NAPL) contamination and also in petroleum recovery where gas is injected into water-oil systems in order to improve oil recovery. In petroleum reservoirs, water-alternating-gas (WAG) injection often recovers oil more efficiently than injection of either gas or water on their own. These three-phase flow processes are further complicated by variations in the wettability state of the porous medium [1–3]. In order to model three-phase flow at the macroscopic scale, it is necessary to determine the associated phase relative permeabilities and capillary pressures. In macroscopic flow models the relative permeability denotes the fluid dependent part of the permeability in Darcy's law, the constitutive law that links the flow rate of a phase to the pressure gradient within that phase. Since measurement of these three-phase quantities is extremely difficult, we may either devise empirical methods or appeal to pore-scale network simulators, which incorporate our understanding of the microscopic physics. The pore-scale behavior in a three-phase system is governed by capillary displacements, which depend on the three interfacial tensions, the wettability or oil-water contact angle at the pore surfaces and the pore size. This paper explores the consequences of various types of system wettability for the pore-scale modeling of three-phase flow.

Variation of the wettability or oil-water contact angle from pore to pore has two major effects on three-phase flow. The first effect relates to the pore occupancies, i.e., which phase occupies which pore, and this in turn affects the dependence of relative permeabilities on saturations. The second effect relates to the presence or absence of wetting films along the pore walls, which has large consequences for the continuity of the phases throughout the porous medium. Van Dijke *et al.* [4,5] and van Dijke and Sorbie [6] have developed an analytical model for all possible three-phase occupancies in a fully accessible capillary bundle model of arbitrary wettability. In these systems the values of the oil-water contact angles may be correlated to pore sizes, e.g., small pores water-wet and large pores oil-wet, or uncorrelated such as in fractionally-wet systems, where water-wet and oil-wet pores of all sizes exist. Furthermore, for each pore size, values of the contact angles may be randomly distributed. It turns out that a three-phase force balance or ''constraint'' equation fixes the wetting order of the phases for a given oil-water contact angle and set of interfacial tensions [7,8]. This results in a fairly restrictive set of physically possible pore occupancies which are in turn linked to the saturation dependencies of the three-phase relative permeabilities and capillary pressures as discussed in detail in Ref. [5].

In uniformly water-wet porous media, it is generally found that the gas and water relative permeabilities depend only on their own saturations and resemble the corresponding two-phase relative permeabilities in gas-oil and water-oil systems, respectively. On the other hand, the oil relative permeability depends on two saturations and is assumed to be

*Electronic address: rink@pet.hw.ac.uk

some combination of the two corresponding two-phase relative permeabilities. In pore-scale terms, water occupies the small pores, gas occupies the large pores and the ''intermediate-wetting'' oil phase occupies the medium sized pores ''between'' water and gas. This pore-scale view was the basis for the widely used Stone water-wet empirical models for three-phase relative permeabilities [9,10]. However, in systems that are not uniformly wetted, all three phases may be the intermediate-wetting phase in different regions of the saturation space [4,5]. Furthermore, when the values of the contact angles are randomly distributed, regions exist where the relative permeabilities of all three phases depend on more than one saturation [6]. For each system it can be demonstrated how the three-phase relative permeabilities relate to the corresponding two-phase relative permeabilities, or it is shown that such a relation does not exist at all.

Since the analytical capillary bundle model referred to above [4,5] is fully accessible, no phase trapping or hysteresis effects are reproduced. Hence, a three dimensional (3D) interconnected network model is necessary to incorporate these phenomena, as well as incorporating the additional effect of wettability, the presence or absence of wetting films. Existing three-phase network simulators [11–14], focus mainly on strongly water-wet or oil-wet systems. In these systems films of the wetting phase are present throughout the network, therefore it is assumed that this phase is continuous to the outlet. Laroche *et al.* [15] have developed a network simulator for 2D systems with geometrical patterns of strongly water-wet and strongly oil-wet pore clusters. In these systems the continuity of the wetting phase in a particular pore cluster is determined by its connectivity to inlet or outlet. However, for weakly wetted media wetting films of the wetting phase may not exist at all and the overall continuity of the wetting phase vanishes. For example, water-wetting films vanish when the oil-water contact angle is less than approximately 45°, depending on the details of the pore geometry [16,17]. Additionally, continuity of oil depends on the existence of (spreading) layers in gas-filled water-wet pores. In general, phase continuity also depends on the dimensionality of the network (2D or 3D), the coordination number (z) and the number of phases in the network. Although, according to percolation theory [18], in a 3D porous network one of the phases is likely to form a cluster that is connected to both the inlet and the outlet, a significant number of clusters of the remaining phases may exist which are disconnected from both inlet and outlet, but not trapped. The presence of disconnected clusters can be observed from various three-phase micromodel experiments even under strongly water-wet conditions [19–24]. We demonstrate in this paper that the presence of disconnected clusters has major consequences for the displacement mechanisms as well as for the choice of outlet boundary conditions.

In Sec. II we describe the 3D three-phase network model, which can perform any arbitrary cycle of phase injections. A number of benchmark simulations for systems with nonuniform wettability, mixed-wet with the larger pores oil-wet (MWL), are presented in Sec. III. The outcome of these simulations is presented as phase paths in saturation space and in the form of pore occupancy histograms and histograms of the type of displacements. First, we compare the simulated saturation paths with those of the analytical capillary bundle model. Then, we show the saturation paths and occupancy and displacement statistics for a number of WAG simulations, which bring out the various features of the model, in particular, those related to the wettability. In this paper we focus on the displacement mechanisms and saturation paths, and we have not attempted to extract relations for capillary pressures and relative permeabilities, as discussed in Sec. IV.

Finally, we acknowledge that considerable progress has been made in understanding the detailed physics of phase distributions in corners of pores with noncircular cross section expressing film flow, see e.g., Refs. [25,26], and of wettability variations within a single pore [27,28]. Detailed film flow has not yet been included in our model, which means that we cannot make fully quantitative predictions. However, we implicitly represent films in our model by allowing continuity along a pore of phases other than the phase occupying the bulk of the pore, which is expected to be sufficient for the qualitative results reported.

II. DESCRIPTION OF THE NETWORK MODEL

The main features of our three-dimensional network simulator for general three-phase immiscible incompressible flow in porous media of arbitrary wettability are as follows:

(1) The model consists of a rectangular network of capillary elements (pores) of randomly distributed sizes e.g., these may be tubes (circular, triangular, etc.) or any other analysable ''pore'' geometry. Sites at the nodes of the network are not explicitly represented in the model. The coordination number z can be varied by randomly removing a certain fraction of pores. Pore sizes may be specified according to a variety of random distributions, including uniform, log uniform, exponential, power law, Rayleigh, etc.

(2) Each pore may be water-wet or oil-wet to a certain degree (wettability), specified by the cosine of the oil-water contact angle θ_{ow}. Pores are water-wet if $0 \leqslant \cos\theta_{ow} \leqslant 1$ and oil-wet otherwise. From the latter the gas-oil θ_{go} and gas-water θ_{gw} contact angles are computed as [5]

$$\cos\theta_{go} = \frac{1}{2\sigma_{go}}\{C_{S,o}\cos\theta_{ow} + C_{S,o} + 2\sigma_{go}\}, \tag{1}$$

$$\cos\theta_{gw} = \frac{1}{2\sigma_{gw}}\{(C_{S,o} + 2\sigma_{ow})\cos\theta_{ow} + C_{S,o} + 2\sigma_{go}\}, \tag{2}$$

where σ_{ow}, σ_{go}, and σ_{gw} denote the equilibrated interfacial tensions and $C_{S,o}$ is the oil spreading coefficient: $C_{S,o} = \min(0, \sigma_{gw} - \sigma_{go} - \sigma_{ow})$. Relations (1) and (2) are consistent with the equation of Bartell and Osterhof [7], and van Dijke and Sorbie [29] describe the consequences of the latter in more detail.

(3) The cosines of the oil-water contact angles θ_{ow} are randomly distributed, but correlated to pore size r, as follows. The cosines that take values c obey the probability density function

$$f(r,c)=f^{+}(c)\cdot g(r)+f^{-}(c)\cdot[1-g(r)], \tag{3}$$

where f^{+} and f^{-} are separate density functions for water-wet and oil-wet pores, respectively, and $g(r)$ is a "tapering" function. For example, for a distribution where the smaller pores are water-wet and the larger oil-wet, but with a range of intermediate sizes for which pores are both water-wet and oil-wet, $g(r)$ equals 1 for pore sizes corresponding to water-wet pores only and 0 for pore sizes corresponding to oil-wet pores only. For pore sizes corresponding to both water-wet and oil-wet pores we take $g(r)$ linearly decreasing from 1 to 0. The functions f^{+} and f^{-} are taken as power laws of the form $f(c)=K\cdot(1-|c|)^{n}$ for $c_1<c<c_2$ and 0, otherwise. The power is $n\geqslant 0$, where $n=0$ yields the uniform distribution, c_1 and c_2 denote the minimum and maximum attained values of $\cos\theta_{ow}$ and K is a normalization constant.

(4) The degree of wettability of a pore determines the presence of a film of water or oil at the pore wall, ensuring continuity of the film phase along the pore. Therefore, for water-wet pores we specify a threshold value such that water films are present for $\cos\theta_{ow}$ above the threshold and for oil-wet pores we specify a second threshold value such that oil films are present for $\cos\theta_{ow}$ below the threshold. Furthermore, for a spreading oil, i.e., when $C_{S,o}=0$, a gas-filled water-wet pore has an oil spreading layer that ensures continuity of oil along the pore. Notice, that for a nonspreading oil we do not include oil layers between gas and water in a water-wet pore, which is sometimes assumed in network models with more detailed pore geometries [11–14].

(5) Invasion of a phase occurs by invasion-percolation principles and flow is assumed to be dominated by capillary forces. During one invasion step a chain of one or more displacements occurs, involving clusters of the various phases as explained in point 7 below.

(6) In each pore displacements of one phase by another may occur pistonlike or by snap-off. The corresponding capillary entry pressures are given by the Young-Laplace equation for the three-phase combinations $ij=ow,go,gw$,

$$P_{c,ij}=\eta\frac{\sigma_{ij}\cos\theta_{ij}}{r}, \tag{4}$$

where $\eta=1$ applies to snap-off and $\eta=2$ to pistonlike displacements. Snap-off can only occur if the more wetting phase is invading (imbibition), if the targeted pore has a film or layer of that phase and when continuity to the considered pore exists through films or layers from the inlet or from a pore that is bulk filled with the imbibing phase. Observe that our imbibition algorithm is rather simple and neglects, for example, the gradual transition to total absence of snap-off for increasingly weakly wetted pores, as well as the so-called cooperative filling in imbibition, as proposed by Lenormand and Zarcone [30]. However, our model retains the qualitative features that pistonlike displacement is favored over snap-off and that snap-off can occur only in the presence of films or layers of the imbibing phase.

(7) In particular, when wetting films are absent, clusters of each phase may be disconnected from the inlet or outlet but not necessarily be trapped, as sketched in Fig. 1. Such clusters can only move by multiple displacements, i.e., injection of the invading phase triggers a chain of interface displacements throughout the network involving a series of phase clusters spanning from inlet to outlet. These chains are an extension of the often described double displacements, see e.g., Refs. [13,14,31]. Multiple displacement chains have been observed during experiments described by Sohrabi *et al.* [23,24] and the modeling of some of this experimental work has been described by van Dijke *et al.* [32]. To determine the most likely displacement, we must first find the pore with lowest capillary entry pressure for each cluster-cluster interface. Then, for each possible chain of clusters, the target pressure difference P_{ij}^{target} between the pressure P_i^{in} of the invading phase and the pressure P_j^{out} of one of the remaining phases at the outlet is found as $(i,j,k=o,w,g)$

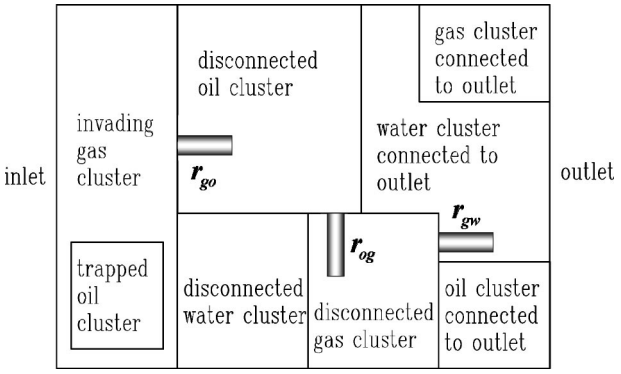

FIG. 1. Map of phase clusters in the network showing their connectivity to inlet or outlet. A possible displacement chain occurs through the indicated pores at cluster-cluster interfaces.

$$P_{ij}^{\text{target}}=P_{c,ik}^{\text{eff}}+P_{kj}^{\text{out}}, \tag{5}$$

where $P_{c,ik}^{\text{eff}}$ represents the sum of the capillary entry pressures for the involved clusters. $P_{kj}^{\text{out}}=P_k^{\text{out}}-P_j^{\text{out}}$ denotes the difference between the pressure in the outlet connected cluster in the chain, with phase k, and the pressure in the chosen outlet phase. For example, a triple displacement chain for gas injection through the pores indicated in Fig. 1 includes gas (at the inlet) displacing oil from pore r_{go}, then oil displacing gas from r_{og} and then gas displacing water from r_{gw} through the outlet, shortly $g\rightarrow o\rightarrow g\rightarrow w$. Taking oil as the reference phase at the outlet, the target is P_{go}^{target} such that $P_{c,gw}^{\text{eff}}=P_{c,go}(r_{go})-P_{c,go}(r_{og})+P_{c,gw}(r_{gw})$ and P_{wo}^{out} is imposed at the outlet. Of all possible displacement chains the one with minimum P_{ij}^{target} is carried out and to achieve this, a shortest-path tree-search algorithm has been implemented. This algorithm is very computationally intensive, especially if long displacement chains (say longer than 6 clusters) are allowed. Notice that in each pair of phase indices i,j,k in Eq. (5) the phases may occur in any order and the indices may even be identical, although at the outlet we would have $P_{kk}^{\text{out}}=0$ by definition.

(8) Gravity effects are included by adding a buoyancy term $P_{c,ij}^{\text{grav}}(r_{ij})=-\Delta\rho_{ij}\cdot(h^{\text{out}}-h_{ij})$ to each capillary entry pressure occurring in a chain of displacements. g is gravitational acceleration, $\Delta\rho_{ij}=\rho_i-\rho_j$ denotes the density differ-

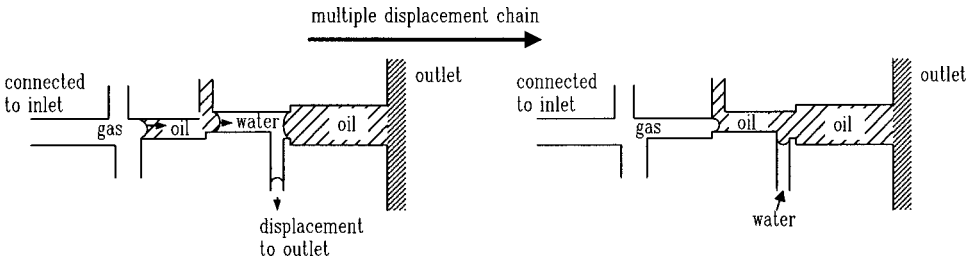

FIG. 2. Multiple displacement chain during gas injection, for which a disconnected oil cluster reconnects to an outlet connected oil cluster.

ence between the invading phase i and the defending phase j at the considered pore, which has size r_{ij} and height h_{ij} relative to the height of the outlet h^{out}.

(9) At the boundaries perpendicular to the inlet/outlet direction, periodic boundary conditions are imposed to minimize effects of these boundaries on the flow patterns. At the inlet boundary the invading phase pressure is specified, where no-flow conditions apply to the remaining phases.

(10) At the outlet boundary, pressures are imposed for each phase that is present at the outlet, through the pressure differences P_{kj}^{out}. The P_{kj}^{out} may be kept constant during a flood, i.e., external pressures are applied, where the network is considered to represent an entire micromodel or core. On the other hand, the P_{kj}^{out} may vary with the displacements within the network, reflecting the view that the network represents only a small part of a reservoir. Specifically, when a disconnected cluster reconnects to the outlet, the pressure of the reconnecting cluster is consistent with the latest chain of displacements and reflects more accurately the pressure of that phase than the already imposed outlet pressure. Therefore, the pressure of this reconnecting cluster is taken as the new outlet pressure for that phase. Notice that Fenwick and Blunt [14] and Lehrdahl *et al.* [33] change the outlet pressures after *all* double displacements, while here pressures change only when during a multiple displacement event the described reconnection takes place. In Fig. 2 the situation is sketched in which a disconnected oil cluster reconnects to an oil cluster that is already connected to the outlet. The pressure in such a reconnecting cluster P_l^{rec} differs from the pressure in the reference outlet phase by

$$P_{lj}^{\text{rec}} = P_{c,lk}^{\text{eff}} + P_{kj}^{\text{out}}. \tag{6}$$

Similar to Eq. (5), $P_{c,lk}^{\text{eff}}$ represents the sum of the capillary entry pressures for the pores involved in the part of the displacement chain stretching between the reconnecting cluster and the cluster at the end of the chain. The outlet pressure differences then change to

$$P_{lk}^{\text{out,new}} = P_{lj}^{\text{rec}} + P_{jk}^{\text{out}} \qquad \text{for } k \neq l. \tag{7}$$

If in the displacement example of point 7 above, the oil cluster reconnects to an oil cluster that was already connected to the outlet, then $P_{oo}^{\text{out,new}} = -P_{c,go}(r_{og}) + P_{c,gw}(r_{gw}) + P_{wo}^{\text{out}}$. Hence, the outlet oil-water pressure difference becomes $P_{ow}^{\text{out,new}} = P_{oo}^{\text{rec}} + P_{ow}^{\text{out}}$, and the oil-gas pressure difference becomes $P_{og}^{\text{out,new}} = P_{oo}^{\text{rec}} + P_{og}^{\text{out}}$.

Only when the invading cluster is connected to the outlet, a no-flow condition is imposed for the invading phase at the outlet. This means that the outlet pressure difference related to the invading phase becomes identical to the target pressure difference. Furthermore, when the described ''constant'' outlet boundary conditions are imposed, the outlet pressure difference between the two phases other than the invading phase (say P_{ow}^{out} during a gas flood) is taken constant, whereas the remaining pressure difference (say P_{go}^{out} during a gas flood) is taken equal to the (historic maximum of the) target pressure difference.

(11) Both two-phase flow and three-phase flow are included and the invading phase can be changed arbitrarily, specifically to model consecutive flood cycles during water-alternating-gas (WAG) processes.

(12) A flow process ends when a designated saturation criterion is met, when displacement chains of less than a specified maximum length are no longer available or when all defending phases have ceased to be continuous to the outlet (both directly and through films or layers). A stricter version of the latter criterion specifies that all defending phases have lost hydraulic connectivity.

(13) The volume of the individual phases is conserved by allowing pores to be fractionally filled with more than one phase. This feature is necessary when in a multiple displacement chain pores with different sizes are involved. A consequence of this mechanism of mass conservation is that in one displacement usually only one pore is completely filled, i.e., over an entire chain, we compute which pore filling requires the smallest phase displacement and partially fill the remaining pores in the chain according to this minimum volume. The fractional filling mechanism can also easily provide for more elaborate saturation calculations based on detailed film configurations, see e.g., Refs. [25,26], although this has not been included in the present model. The fractional filling mechanism also affects subsequent invasion of a pore. We assume that despite fractional filling a pore has only one bulk phase, the defending phase, until the latter is completely displaced. In this way we ensure that after fractional filling during one displacement chain, the same type of displacement is likely to happen during a subsequent chain, at the same capillary entry pressure, in order to completely fill the pore. Hence, we minimize the proportion of fractionally filled pores in the network.

(14) At each stage of the displacement cycle a range of phase displacement statistics is recorded, including phase pore occupancies as a function of pore size, the type of displacement, i.e., ''which phase displaces which,'' snap-off vs pistonlike, for the pore that is completely filled, as indicated in point 13, and the number of displacements involved in a chain. These statistics are presented in Sec. III B.

III. THREE-PHASE SIMULATIONS IN MIXED-WET SYSTEMS

We have run a number of simulations on a 3D network with $24\times16\times16$ nodes, i.e., 24 nodes in the flow direction and 16 nodes in the two directions perpendicular to flow. Pore radii r are distributed uniformly between $r_{\min}=5\ \mu$m and $r_{\max}=25\ \mu$m. The network is mixed-wet with the 50% larger pores oil-wet (denoted MWL), radii $r>15\ \mu$m, and the smaller pores water-wet, with radii $r<15\ \mu$m, unless otherwise indicated. The cosines of the oil-water contact angles are $\cos\theta_{ow}=1$ in the water-wet pores and $\cos\theta_{ow}=-1$ in the oil-wet pores, unless stated otherwise. The volume of the pores, necessary for the saturation calculations, scales linearly with r. Values of the interfacial tensions are fixed as $\sigma_{gw}=48$ mN/m, $\sigma_{ow}=32$ mN/m and $\sigma_{go}=24$ mN/m. Hence, the oil spreading coefficient $C_{S,o}=-8$ mN/m and oil is nonspreading. Furthermore, with $\cos\theta_{ow}=-1$ and the present values of the interfacial tensions Eq. (2) predicts $\cos\theta_{gw}<0$, hence gas is wetting to water in the oil-wet pores. Outlet boundary pressures are varied as described in Sec. II, point 10 and up to five displacements per chain are allowed, unless stated otherwise. The remaining parameters are varied for the various simulation sensitivities as specified in the following sections.

All simulations start with a completely oil filled network in which either water or gas injection is simulated up to a prescribed saturation, yielding a two-phase distribution. In this two-phase system the remaining third phase is injected hence leading to three-phase flow. The details of the three-phase flow regimes which emerge are outlined in the following subsections.

A. Comparison of analytical and network modeling results

1. Analytical results

Van Dijke *et al.* [4,5] have studied the effects of wettability for a very simple representation of the porous medium, i.e., a parallel bundle of (cylindrical) tubes with varying radii and wettability, which are similar to the pores in the present network model. Invasion into this capillary bundle model proceeds according to the same principles as for the network model, although issues such as trapping and snap-off will not occur, because all pores are accessible to the invading phase. Furthermore, because of this complete accessibility, only the constant boundary conditions (see Sec. II, point 10) can be applied, i.e., if during a flood a single phase is injected, the pressures of the remaining phases are fixed, which in turn unambiguously defines the capillary pressure between the latter phases. For the capillary bundle model capillary pressures and relative permeabilities as functions of the saturations can be determined analytically, using explicit expressions for the tube volumes and conductances, where the latter are derived from the Hagen-Poiseuille equations. More importantly, using the capillary bundle model, van Dijke *et al.* [4,5] have shown for which saturation combinations the capillary pressures and relative permeabilities vary only with one saturation or with more than one saturation. These saturation dependencies are based on the underlying phase pore occupancies. As a result, the three-phase saturation space may be divided in up to three different regions related to different saturation dependencies. The regions are distinguished by the directions that the saturation paths take when a single invading phase is injected into a system where the remaining two phases are already present, of which examples are shown in Fig. 3.

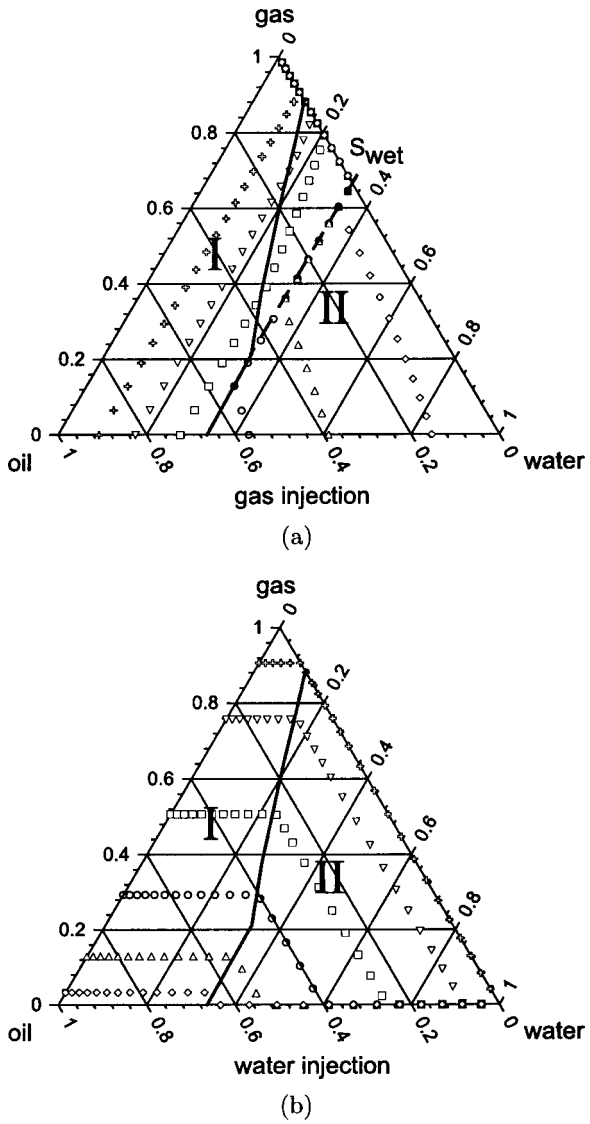

FIG. 3. Saturation paths for the mixed-wet capillary tube model, (a) gas injection paths and (b) water injection paths. The solid line delineates the saturation-dependency regions I and II.

Saturation paths are presented for gas injection into a water-oil system in Fig. 3(a) and for water injection in a gas-oil system in Fig. 3(b), in the mixed-wet capillary tube model with the parameters specified above. For example, the gas injection path in Fig. 3(a) starting at oil saturation $S_o=0.91$ entirely follows a water isosaturation line, indicating that the oil-water capillary pressure depends on the water saturation only. In fact, all paths crossing the indicated region I show this behavior. Similarly, water injection paths in Fig. 3(b) crossing the same region I follow gas isosaturation lines, indicating that the gas-oil capillary pressure depends

on the gas saturation only. Van Dijke *et al.* [4,5] have shown that the combined information from both diagrams indicates that in region I the oil relative permeability depends on two saturations, whereas the water and the gas relative permeabilities each depend on their own saturations only.

On the other hand, gas injection paths crossing through the indicated region II are curved, indicating that the oil-water capillary pressure depends on two saturations, whereas water injection paths are oil isosaturation lines. In region II only the gas relative permeability depends on two saturations. The third region where the water relative permeability depends on two saturations, is absent for the present combination of contact angles and interfacial tensions in which gas is wetting to water in the oil-wet pores. Observe that one path may cross different regions. Notice further that all gas injection paths [Fig. 3(a)] starting at oil saturations smaller than $S_o = 0.67$ end up on the water isosaturation line with saturation $S_w = 0.33$, indicated as S_{wet}, for which water occupies exactly all the water-wet pores. This feature results from the jump in contact angles, hence in capillary pressures, at the pore size separating the water-wet and oil-wet pores, $r = 15\ \mu\text{m}$ [4].

2. Simulations with high phase continuity

In Fig. 4 we present simulation results of gas and water injection processes into the full 3D network model described above, for which the phase continuity is high. High phase continuity is achieved by taking the highest possible coordination number $z = 6$, and assuming that water wetting films are present in the water-wet pores and oil-wetting films are present in the oil-wet pores, i.e., both types of pores are strongly wetted. In this case, we may expect the best possible comparison with the completely accessible capillary tube model. All three-phase paths are continued until both defending phases are no longer able to escape to the outlet, not even through wetting films, leaving their residual saturations. The high phase continuity is obvious from the saturation diagram in Fig. 4(a), as both water and oil residual saturations are virtually zero after the various gas injections. Since the fractions of both water-wet and oil-wet pores, 0.5 each, are well above the percolation threshold of 0.25 for this network [18], these sets of pores are connected throughout the network and let almost all the fluid escape through the respective connected wetting films. On the contrary, the simulation results in Fig. 4(b) show that the gas residual saturations are significant due to the fact that there are no gas wetting films.

Comparison with the analytical results in Fig. 3 shows good agreement. Indeed, in the network results in Fig. 4, region I is clearly distinguishable, where the paths during both gas injection and water injection are virtually all isosaturation lines. Only for the water injection path starting at $S_o = 0.10$ is the simulated path not an isosaturation line due to the fact that only a small number of oil-filled pores are present near the inlet, where water starts invading. Also the boundary between the saturation-dependency regions, taken from the analytical model onto the simulation diagrams, is well reproduced. A significant deviation of the simulated from the analytical results occurs during water injection for low gas saturations, where in the simulations gas becomes trapped.

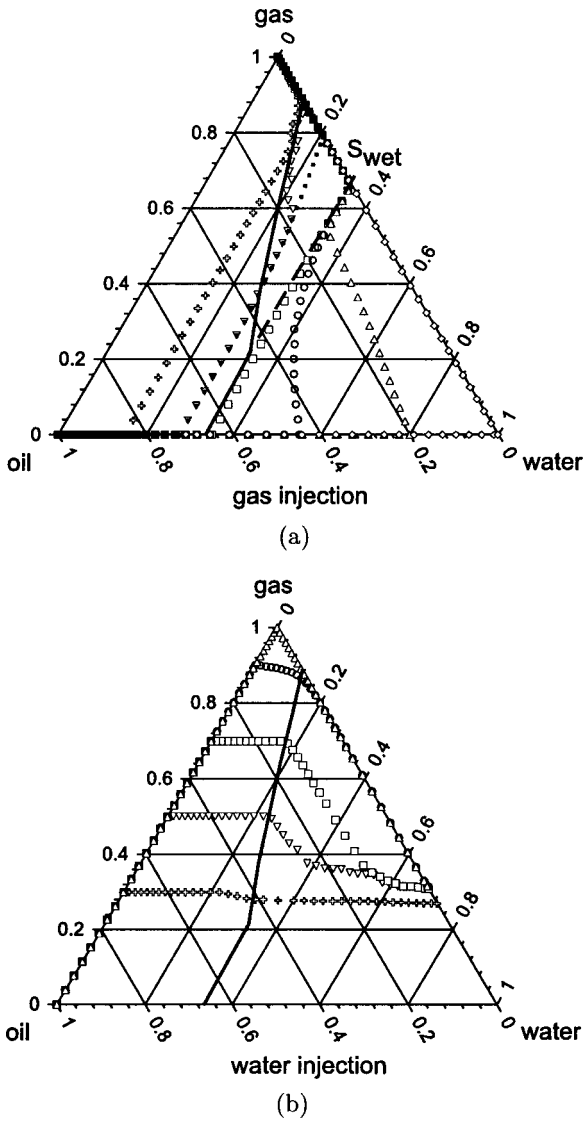

FIG. 4. Saturation paths for the mixed-wet network model with high phase continuity, (a) gas injection paths and (b) water injection paths. The small dots (gas injection starting at $S_o = 0.72$) denote the path with constant outlet pressure difference. The solid line delineates the saturation-dependency regions I and II, as derived analytically.

Another important difference between analytical and simulated results occurs when gas injection paths approach the nonlinear boundary between regions I and the part of region II where $S_w < S_{\text{wet}}$. Interestingly, the simulated paths tend towards this analytically derived curve. Simulations with different sets of parameters have confirmed this behavior. In Fig. 4(a) the gas injection path starting at $S_o = 0.72$ is shown (marked as small dots) when at the outlet boundary instead of varying pressure differences, the constant oil-water pressure difference is imposed, as described in Sec. II, point 10. In region II, this path is different from the varying pressure path and it is much more in agreement with the analytical paths in Fig. 3(a). Additional simulations for both

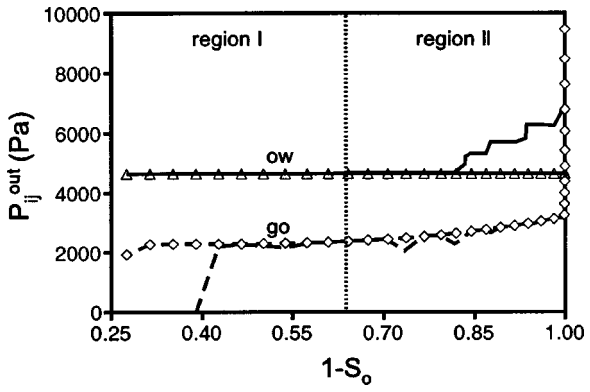

FIG. 5. Oil-water and gas-oil outlet pressure differences for the gas injection simulations with high phase continuity starting at $S_o = 0.72$, when imposing constant (lines with markers) and varying outlet boundary conditions (lines without markers). Additionally, the saturation-dependency regions that are crossed by the saturation path are indicated.

gas and water injections with such constant boundary conditions did not show further deviations in other parts of the saturation space.

To highlight the differences between the gas injection paths with varying and constant boundary conditions we present in Fig. 5 the oil-water and gas-oil pressure differences along the saturation paths as a function of $1-S_o$. When the path goes through region I, until $1-S_o \approx 0.65$, P_{ow}^{out} for the varying conditions remains approximately constant, but changes, tending upwards, when going through region II. In this region a few double displacements occur associated with reconnection of oil to the outlet as described in Sec. II, point 10, which cause significant changes in P_{ow}^{out}. Apparently, these changes are sufficient to alter the path. Observe that the number of reconnections is small due to the high continuity of the oil phase, hence the changes appear as discrete steps in both the saturation diagram, Fig. 4(a), and the pressure plot Fig. 5.

The varying gas-oil outlet pressure difference becomes nonzero when gas becomes hydraulically connected, at $1-S_o \approx 0.40$, whereafter P_{go}^{out} is identical to the target pressure difference, which reveals some small lack of accessibility. The historic maximum of P_{go}^{out} yields this pressure difference for ''constant'' conditions. Notice that in region II, despite the difference in saturation paths the two P_{go}^{out} are virtually identical, which stresses the agreement of both paths with the analytical theory that $P_{c,go}$ is a function of S_o only in this region [4].

With respect to the proposed multiple displacement chains, chains longer than two displacements are rarely observed during these simulations with high phase continuity. As mentioned above, the gas injections show almost only single displacements, with around 0.1% double displacement chains, all of type gas-displacing-oil-displacing-water ($g \rightarrow o \rightarrow w$). The water injections show up to 43% double displacement chains (for the case starting with $S_o = 0.70$), all of type $w \rightarrow g \rightarrow o$, which is easily explained by the formation of a large number of disconnected gas clusters towards the end of the paths. Although some of the latter double displacements do change the gas-oil outlet pressure difference,

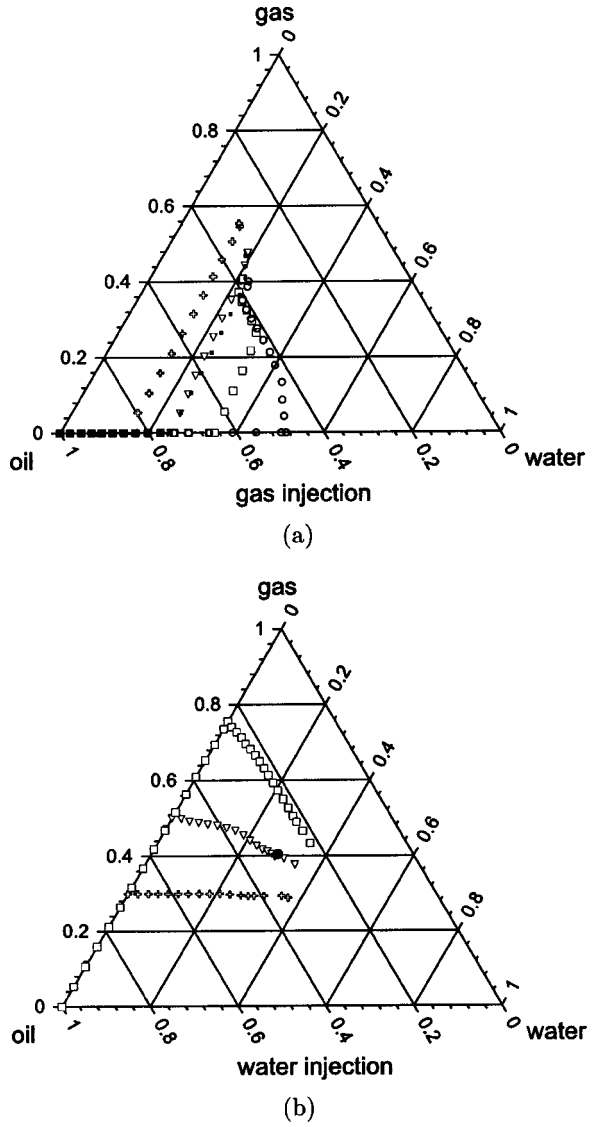

FIG. 6. Saturation paths for the mixed-wet network model with low phase continuity, (a) gas injection paths and (b) water injection paths. The small dots (gas injection starting at $S_o = 0.75$) denote the path with constant outlet pressure difference. The single dot on the water injection path starting at $S_o = 0.50$ indicates the endpoint of this path if only two displacements per chain are allowed.

there has not been a substantial effect on the saturation paths. The pressure variations appear to be only small oscillations around the constant value. Snap-off by water, mainly of oil, has been observed during the water injections, but this accounts for only up to 2% of all displacements.

3. Simulations with low phase continuity

In Fig. 6 we present simulation results of gas and water injection processes in the described 3D network for which the phase continuity is relatively low, which is achieved by taking coordination number $z = 4$ and by suppressing wetting films in both the water-wet and the oil-wet pores. As expected, residual saturations of all phases are high. In each diagram the three-phase path starting at the lowest oil satu-

ration indicates the two-phase flow residual oil saturations, i.e., $S_o=0.49$ after water flooding [Fig. 6(a)] and $S_o=0.24$ after gas flooding [Fig. 6(b)]. Despite the high levels of trapping the gas injection paths of Fig. 6(a) show reasonable agreement with the analytical results of Fig. 3(a), i.e., gas displaces only oil when starting at high oil saturations (region I) and both oil and water when starting at lower oil saturations. Only the water injection paths of Fig. 6(b) starting at intermediate oil saturations show some agreement with the analytical results of Fig. 3(b). For high oil saturations gas trapping dominates the process and for low oil saturation oil trapping dominates the process.

Many double displacements have been observed during these simulations, up to 56% for the gas injection paths and up to 54% for the water injection paths. However, these double displacements do not lead to vast changes in the saturation paths, when taking different outlet boundary conditions. The maximum deviation between varying and constant condition paths is found for gas injection starting at $S_o=0.75$ [marked as small dots in Fig. 6(a)], but the deviation is very small. As for the high phase continuity simulations, the path with constant oil-water outlet pressure difference is more in agreement with the analytical results of Fig. 3(a).

Also a number of multiple displacement chains occur, although mostly for the water injection paths, e.g., 6% of chains have three displacements, 5% have four displacements and 5% have five displacements for the water injection path starting at $S_o=0.24$. These percentages are 5, 11, and 12 for the water injection path starting at $S_o=0.50$. As the latter simulation also involves a very large number of separate phase clusters, 1758 at the end of the simulation in the present system with 12 500 pores, we may expect that the presence of multiple displacement chains has a relatively large impact on the saturation path. Therefore, we have carried out the same simulation, but allowing chains of only up to two displacements to occur. The resulting saturation path is virtually the same as that for five displacements per chain, but ends significantly earlier as marked in Fig. 6(b) by the single dot. For two displacements the path ends at $S_w=0.288$ and $S_o=0.307$, while for five displacements the path ends at $S_w=0.341$ with $S_o=0.282$.

B. Water-alternating-gas simulations

To bring out further the features of our three-phase network model for mixed-wet porous media, we have carried out water-alternating-gas (WAG) simulations as described in the caption of Fig. 7, for four different sets of network parameters. Water and gas are injected subsequently, for the first water and gas floods until the prescribed saturations are reached, as indicated in Fig. 7, and for the second water and gas floods until oil and the remaining defending phase can no longer escape to the outlet, i.e., until they have become residual. Notice, that some of the oil that has become residual after the second water flood may still be displaced during the second gas flood, which is precisely why WAG injections are carried out. We discuss in detail the base case simulation, which has the same parameters as the low-phase continuity simulations in Sec. III A, i.e., a mixed-wet network with no wetting films in either water-wet or oil-wet pores and coordination number $z=4$. Then, we discuss the remaining three cases which differ from the base case with respect to the wettability parameters. In Fig. 7 the saturation paths for the various WAG simulations are shown and in Table I the residual oil saturations after the first gas flood and the second water and gas floods are listed.

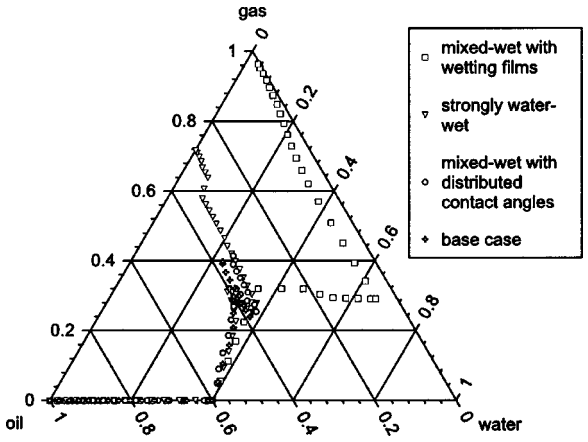

FIG. 7. Saturation paths for the various WAG simulations. Starting at 100% oil, 40% water is injected, then 32% gas, then water until residual and then gas until residual.

In the simulation denoted ''mixed-wet with wetting films,'' water and oil wetting films are present in the water-wet and oil-wet pores, respectively, contrary to the base case. The ''strongly water-wet'' simulation has been carried out on the same network as the base case but with all pores water-wet, $\cos\theta_{ow}=1$, and water wetting films are present in all pores. In the ''mixed-wet with distributed contact angles'' simulation the cosines of the contact angles are not constant as in the base case, but are uniformly distributed between 0 and 1 for the water-wet pores and between -1 and 0 for the

TABLE I. Residual oil saturations after the first gas flood $S_{or,g1}$, after the second water flood $S_{or,w2}$ and after the second gas flood $S_{or,g2}$ for the various simulations.

	Base case	Mixed-wet with wetting films	Strongly water-wet	Mixed-wet with distributed contact angles
$S_{or,g1}$	0.398	0.327	0.399	0.381
$S_{or,w2}$	0.387	0.053	0.374	0.364
$S_{or,g2}$	0.375	0.005	0.282	0.341

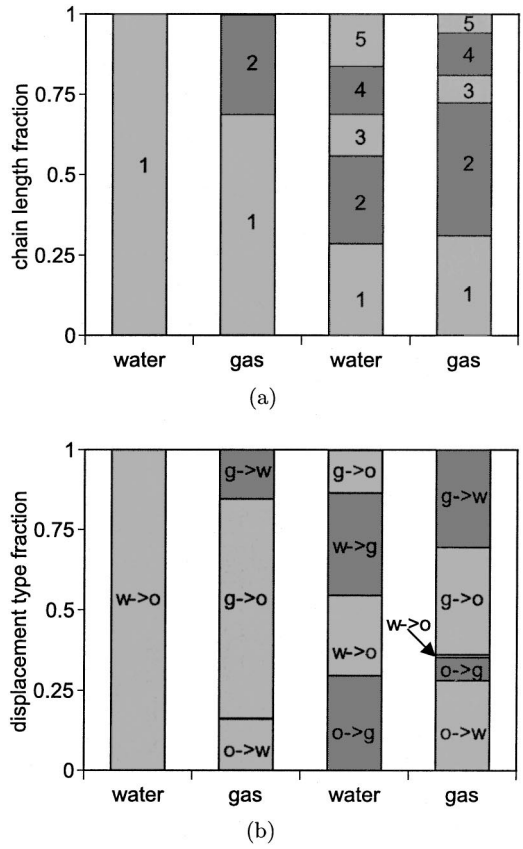

FIG. 8. Displacement statistics for consecutive floods in the WAG base case simulation, (a) fraction of the total number of displacement chains with the indicated length: single (1), double (2), etc., and (b) fraction of the total number of chains with the indicated type of displacement (e.g., $g \rightarrow o$ indicates gas displacing oil).

oil-wet pores. As in the base case, no wetting films are present for the latter simulation.

1. Base case WAG simulation

The base case WAG saturation path in Fig. 7 shows considerable oil production during the first gas flood, as for the single gas injections shown in Fig. 6(a). During the second water and gas floods the path lies slightly outside the envelope of single gas injection curves and there is merely an exchange of gas and water and not much additional oil recovery.

To investigate the displacement processes taking place during the various floods of the WAG base case, histograms of the length of the displacement chains and of the type of displacements are presented in Fig. 8. Note that in each chain only the type of displacement is recorded for the pore that is exactly filled by the incoming phase as described in Sec. II, point 14. Figure 8(a) shows that during the first water flood only single displacement chains have occurred, whereas Fig. 8(b) indicates that these are all of type $w \rightarrow o$, obviously. During the first gas flood single displacements of types $g \rightarrow o$ and $g \rightarrow w$ have taken place. The recorded double displacement chains are of type $g \rightarrow o \rightarrow w$ in view of the recorded $o \rightarrow w$ displacements, although a tiny fraction $w \rightarrow o$ displacements may suggest a few $g \rightarrow w \rightarrow o$ chains as well.

During the second water and gas floods many triple and higher-order displacements have been recorded as shown in Fig. 8(a). During the second water flood about 20% of the displacements are of $w \rightarrow o$ type and about 10% are of $g \rightarrow o$ type, whereas Fig. 7 shows little oil production during this flood. Therefore, most of these displacements are part of double or multiple chains and oil is present mostly in disconnected clusters. The overall gas production shows that part of the gas phase is continuous to the outlet, although the occurrence of multiple displacements requires disconnected gas clusters as well. On the other hand, no $o \rightarrow w$ or $g \rightarrow w$ displacements have been recorded, hence no disconnected water clusters come into the displacement chains, indicating high continuity of the water phase. As a result, most higher-order displacement chains in the second water flood start with water, followed by a string of oil and gas clusters, and end with gas, as in a fivefold chain like $w \rightarrow g \rightarrow o \rightarrow g \rightarrow o \rightarrow g$.

During the second gas flood again little oil has been produced, therefore the recorded $g \rightarrow o$ displacements are part of double or multiple chains and the oil phase is highly discontinuous, although still mobile. As only a tiny fraction $w \rightarrow o$ and no $w \rightarrow g$ displacements are recorded, the continuity of water remains probably high and only few multiple displacement chains contain water clusters, such as $g \rightarrow w \rightarrow o \rightarrow g$, although many chains may end with a water cluster. Notice that the latter chain ends with a gas cluster, which is possible in view of the recorded $o \rightarrow g$ displacements when the invading gas phase is not yet hydraulically connected. According to the recorded fractions in Fig. 8(a), we find that many single $g \rightarrow w$ and double $g \rightarrow o \rightarrow w$ chains occur, whereas most multiple displacement chains are of type $g \rightarrow o \rightarrow g \rightarrow w$, i.e., a string of gas and oil clusters ended by a water cluster.

An additional simulation with the base case parameters, but allowing only two displacements per chain, similar to the single water flood described in Sec. III A 2, has not given very different results, except in the chain length histogram. Interestingly, the residual oil saturation after the second water flood is slightly higher, but after the second gas flood is slightly lower than in the base case simulation.

The pore occupancy histograms of Fig. 9 offer a different outlook on the displacements that have taken place during the base case WAG simulation, as they show the actual distribution over the sets of pores with different sizes and wettabilities. At the end of the first water flood [Fig. 9(a)] water has displaced virtually all oil from the water-wet pores ($r < 15\ \mu$m) and has started displacing oil from the largest oil-wet pores onwards. The sharp division between water-filled and oil-filled pores indicates high continuity of both oil and water phases.

The first gas flood has clearly displaced mostly oil, which follows from comparison of Figs. 9(a) and 9(b), although the blurred divisions between the phases indicates significant reduction of the oil phase continuity. Gas has displaced not only oil from the oil-wet pores, but also (simultaneously) water from the water-wet pores, in agreement with the analytical results for this type of porous medium [4,5]. Moreover, some of the larger water-wet pores have been refilled with oil as a result of double $g \rightarrow o \rightarrow w$ displacements, re-

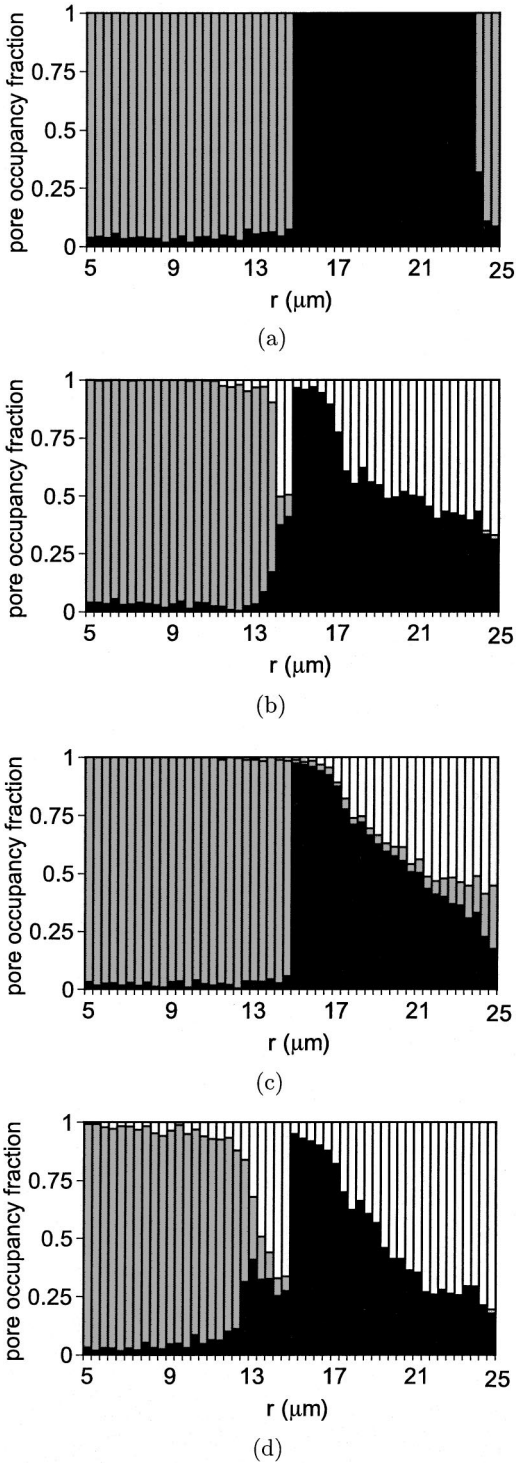

FIG. 9. Pore occupancy statistics during the base case WAG simulation at the end of (a) the first water flood, (b) the first gas flood, (c) the second water flood and (d) the second gas flood (black represents oil, gray represents water, white represents gas).

corded in the histogram of Fig. 8(a).

Figure 9(c) shows that the second water flood has displaced both oil and gas from the water-wet pores before entering the largest oil-wet pores, which is again in agreement with the analytical findings. At this stage, the continuity of both oil and gas phases has become low, as water has not

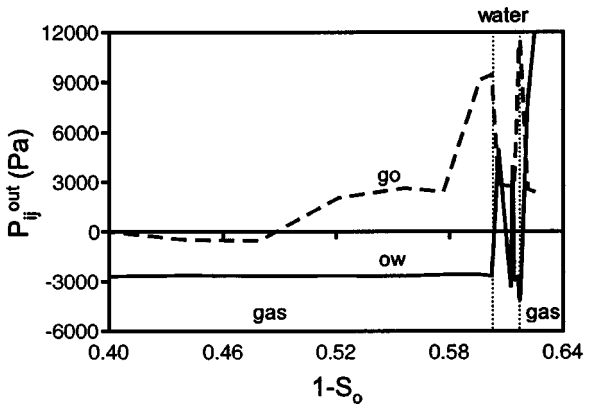

FIG. 10. Oil-water and gas-oil outlet pressure differences for the indicated first gas, second water, and second gas floods in the base case WAG simulation.

uniformly filled the oil-wet pores from the largest onwards, but is spread out over oil-wet pores of all sizes. Observe that some ranges of oil-wet pores contain more oil than before this flood as a result of higher-order displacement chains.

The occupancy histogram after the second gas flood in Fig. 9(d) shows a pattern similar to that after the first gas flood in Fig. 9(b). Little oil has been produced, but again a significant amount has ended up in the water-wet pores. Since also the water phase has become discontinuous at the end of this flood, gas occupies water-wet pores of all sizes.

Figure 10 shows the oil-water and gas-oil outlet pressure differences during the base case WAG simulation as a function of $1-S_o$ during the floods following the first water flood. Note that the representation here is not ideal as the variation in oil saturation is small during the second water and gas floods. Furthermore, the actual number of oscillations is often larger than shown.

During the first gas flood, P_{ow}^{out} remains virtually constant although small oscillations associated with oil reconnections do occur. Its value is negative and consistent with the pore occupancy at the end of the first water flood [Fig. 9(a)] where the division between water-filled and oil-filled pores lies in the oil-wet pores, which have negative capillary entry pressures $P_{c,ow}$. During the second water flood P_{ow}^{out} merely reflects the target pressure difference P_{gw}^{target} as water is the invading phase and is probably hydraulically connected. It becomes positive when water invades the water-wet pores filled with oil and gas after the first gas flood [see Fig. 9(b)], but soon becomes negative again, with the occasional oscillation in between, when invading the oil-wet pores. During the second gas flood, P_{ow}^{out} becomes positive again when gas starts invading a significant number of water-wet pores. On average, P_{ow}^{out} is in agreement with the division between oil-filled and water-filled pores in the pore occupancies in a completely accessible model [4,5], although this division is very much obscured by the lack of accessibility.

The gas-oil outlet pressure difference becomes identical to the target pressure difference (see Sec. II, point 10) for $S_o \approx 0.50$ during the first gas flood. Only then the gas phase becomes connected to the outlet and the value of P_{go}^{out} is meaningful. Thereafter, P_{go}^{out} remains positive, which is con-

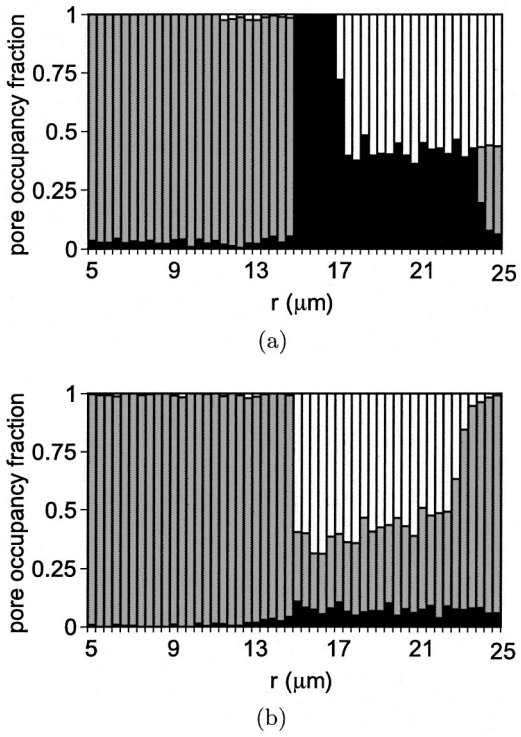

FIG. 11. Pore occupancy statistics for consecutive floods for the WAG simulation ''mixed wet with wetting films'' at the end of (a) the first gas flood and (b) the second water flood (black represents oil, gray represents water, white represents gas).

sistent with the capillary entry pressures $P_{c,go}$ that are positive for all water-wet and oil-wet pores as Eq. (1) shows. P_{go}^{out} during the second water and gas floods shows so many oscillations, as a result of lack of phase continuity, that any further relevant observations are not possible.

An additional simulation with the base case parameters, but with constant outlet boundary conditions as in Sec. II, point 10, did not give very different results. Probably, the choice of outlet boundary conditions is not very important in the presence of many disconnected clusters or the present WAG path lies in a region of the saturation space, where the conditions do not matter, as for the single gas floods described in Sec. III A.

2. Additional simulations with altered wettability

The WAG simulation in a mixed-wet system with both water and oil wetting films present, for which the saturation path is shown in Fig. 7, is characterized by high continuity of the water and oil phases. Similar to the simulations in Sec. III A 1, the fractions of both water-wet and oil-wet pores are above the percolation threshold, here 0.375 for $z=4$ [18]. As a result, the displacement statistics show virtually no higher-order displacements and only a significant percentage of double displacements during the second water flood, when the continuity of the gas phase is low.

The occupancy histogram after the first gas flood in Fig. 11(a) shows a sharp division between the gas and oil occupancy due to the high continuity of the oil phase. The even distribution of oil-wet pores left with water show that gas has

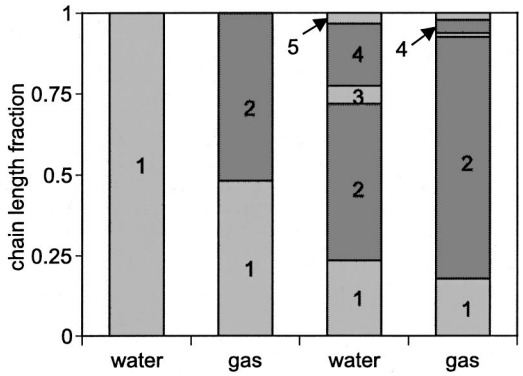

FIG. 12. Histogram of the fraction of the total number of displacement chains with the indicated length in the strongly water-wet WAG simulation.

not been able to reach all pores with the corresponding sizes. The occupancy histogram after the second water flood in Fig. 11(b) indicates that a large amount of gas and a small amount of oil have become trapped, virtually all in the oil-wet pores as those are the last to be invaded by water. This occupancy histogram shows that for the current set of interfacial tensions and contact angles gas is wetting to water in the oil-wet pores as gas occupies generally smaller oil-wet pores than water. Notice that in a large part of the smaller oil-wet pores the oil visible in the histogram of Fig. 11(a) has been replaced by gas through double $w \rightarrow g \rightarrow o$ displacements.

An interesting feature of the histogram of Fig. 11(b) is the non-negligible amount of oil trapped in the oil-wet pores after the second water flood, despite the existence of a connected set of pores with oil wetting films. The reason is probably that this oil is completely surrounded by gas, which in turn is surrounded by water and can therefore not be displaced by capillary mechanisms. However, the saturation path in Fig. 7 indicates that this oil is eventually displaced during the second gas flood.

The residual oil saturations in Table I show immediately that a strongly water-wet system cannot be swept as effectively as a mixed-wet system with wetting films, because in the latter oil can escape through these films. Observe from the chain length histogram of Fig. 12 that in a strongly water-wet system a significant number of higher-order displacements may occur, mostly during the second water flood. Obviously, the multiple displacement chains consist of gas and oil clusters with a possible water cluster only at the beginning or the end.

The differences between the WAG simulation with distributed contact angles and the base case simulation are best understood from the pore occupancy histograms in Fig. 13. After the first water flood (not shown) water has not filled the oil-wet pores from the largest onwards as in the base case, but has invaded oil-wet pores of all sizes simultaneously. This occurs because a number of oil-wet pores of all sizes have contact angles close to $\pi/2$, hence according to Eq. (4) their capillary entry pressures are close to zero and therefore almost insensitive to pore size. The same effect is visible after the second water flood in the histogram of Fig. 13(a), although it partly overlaps with the effect of low oil and gas

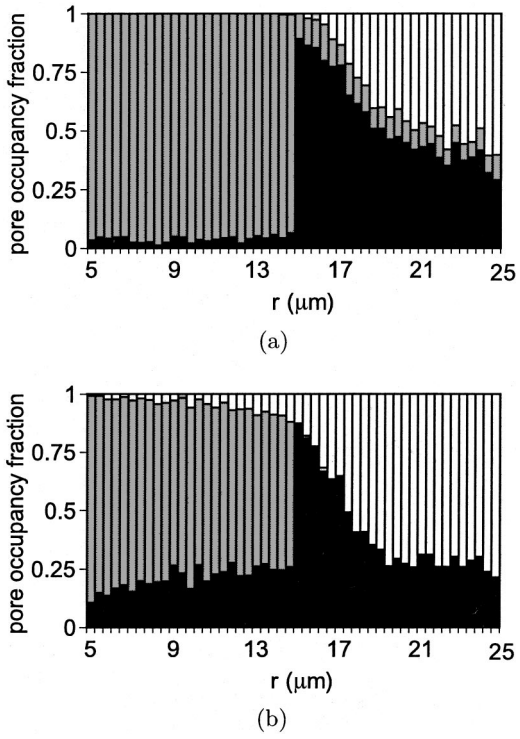

FIG. 13. Pore occupancy statistics for consecutive floods for the WAG simulation ''mixed wet with distributed contact angles'' at the end of (a) the second water flood and (b) the second gas flood (black represents oil, gray represents water, white represents gas).

phase continuity as shown for the base case in the histogram of Fig. 9(c). More strictly, for contact angles close to $\pi/2$ water has to occupy oil-wet pores smaller than gas and larger than oil and for contact angles close to π, water has to occupy oil-wet pores larger than gas [see Eq. (2)]. On the other hand, in a significant number of water-wet pores of all sizes oil has displaced water during the second gas flood, as shown in the histogram of Fig. 13(b), because many of these pores also have contact angles close to $\pi/2$. Finally, the distribution of contact angles has a significant effect on the saturation paths, Fig. 7, and therefore on the recovery, Table I.

IV. DISCUSSION

The implementation of wettability variation from pore to pore in the current network simulator has raised two important issues related to the resulting reduced phase continuity: the existence of so-called multiple displacement chains and the imposition of appropriate outlet boundary conditions. These issues come on top of the range of saturation dependencies of the relative permeabilities and capillary pressure that have become apparent from study of a completely accessible model with varying wettabilities [4–6].

Simulations for 3D networks with realistic connectivities have shown that multiple displacement chains do occur, in particular, during WAG processes, although not exclusively, as the water injection simulations of Sec. III A 2 have shown. However, the impact of these multiple chains on the saturation paths seems to be limited as simulations with different allowed chain lengths have shown. It is not clear yet if this is an intrinsic result or purely caused by the computational limitations, i.e., the restriction on the maximum chain length and the network size. Further analysis for larger chain lengths and network sizes, in combination with percolation theory, may reveal the correlations between these quantities and the saturation path. From the present simulations it has become clear that the number of clusters can be very large for low phase continuity, which is a necessary condition for the existence of multiple chains.

The variations in outlet boundary pressure differences as implemented in this model do occur when multiple displacements take effect and phase reconnections with the outlet take place. However, if the phase continuity is still relatively high, the variations may only appear as small fluctuations around a constant state, as for P_{ow}^{out} during the first gas flood shown in Fig. 10, and have little effect on the subsequent process. On the other hand, it seems that large variations in a situation with low phase continuity also have a small effect, as subsequent displacements are more governed by lack of accessibility than by the boundary conditions. Nevertheless, the simulations with high phase continuity have shown that a small number of reconnections can lead to large variations in pressure difference, which in turn cause significant deviations of the saturation path. In particular, the latter issue requires further investigation as it appears to be related to particular regions in saturation space that have been distinguished previously [4,5], on the basis of the saturation dependencies of the capillary pressures and relative permeabilities in a completely accessible model.

The varying or constant boundary conditions not only affect the saturation paths, but also raise the question of which type of outlet boundary pressure differences realistically represents the capillary pressures of the network. As discussed in Sec. II, point 10, when the network is supposed to represent a small sized porous medium for which the pressures can be externally fixed, such as a micromodel, the constant boundary conditions seem appropriate. When the network is considered to be a part of a large-scale simulator, the varying conditions appear to be more realistic, since pressures should not be imposed externally, but be consistent with the phase interfaces inside the medium. Furthermore, since the dependence of capillary pressure on saturation is directly related to the dependence of relative permeability on saturation it is also vitally important to impose boundary conditions for the outlet pressure differences that are as realistic as possible. Indeed, the question raised by Mani and Mohanty [13] of which pressure difference represents the correct capillary pressures of the network and how to calculate the correct relative permeabilities in systems with low phase continuities, is still unanswered.

To investigate fully three-phase flow in mixed-wet porous media, additional sensitivity studies have to be carried out related to the wettability in combination with fluid parameters, for example, with respect to the distribution of contact angles in relation to the interfacial tensions and with respect to the presence of spreading layers and pore corner films. These studies are currently in progress and will be reported upon in the future.

V. CONCLUSIONS

The present pore-scale network simulator is able to model capillary-dominated three-phase flow in porous media of arbitrary wettability. Simulations for 3D mixed-wet network models have been carried out to investigate the effects of variable wettability and to study the displacement mechanisms in three-phase flow. Two central quantities for analysing the displacement mechanisms are the phase occupancy statistics and the monitoring of multiple displacement chains. Conclusions from the simulations are as follows:

(1) Simulated three-phase saturation paths in systems where there is high phase continuity show good agreement with paths for an analytical completely accessible model [4,5]. As expected, discrepancies arise when the continuity of one or more of the phases decreases as a result of the absence of wetting films or a lower network coordination number.

(2) The network model predicts that multiple displacement chains occur in three-phase processes. These are observed during single three-phase floods, but more profoundly during WAG floods, even in a strongly water-wet system. In some cases, multiple displacement chains lead to more oil recovery compared with allowing only double displacements, but in other cases they lead to less.

(3) Reconnections of disconnected phase clusters to the outlet take place where there is reduced phase continuity and there are multiple displacements. The resulting variations in the outlet boundary pressure differences have an effect in regions of the saturation space that are defined by the analytical model.

(4) Cycles of gas and water injection cause significant breakup of the gas and oil phase clusters in the network. However, higher flooding cycles do not give much additional oil recovery, although the disconnected oil phase is mobile and is moved through the network.

ACKNOWLEDGMENTS

The authors would like to thank S. R. McDougall for supplying the original code of the simulator. The following members of the Heriot-Watt WAG Consortium are acknowledged for supporting this research: The UK Department of Trade and Industry, BP, Shell, PDVSA, BHP, TotalFinaElf, Norsk Hydro and Statoil.

[1] F. Kalaydjian, O. Vizika, J.-C. Moulu, and P.K. Munkerud, in *New Developments in Improved Oil Recovery*, edited by H. J. de Haan (Geological Society, London 1995), Vol. 84, p. 63.
[2] G.R. Jerauld and J.J. Rathmell, SPE Reservoir Eng. **12**, 58 (1997).
[3] O. Vizika and J.-M. Lombard, SPE Reservoir Eng. **11**, 54 (1996).
[4] M.I.J. van Dijke, S.R. McDougall, and K.S. Sorbie, Transp. Porous Media **44**, 1 (2001).
[5] M.I.J. van Dijke, K.S. Sorbie, and S.R. McDougall, Adv. Water Resour. **24**, 365 (2001).
[6] M.I.J. van Dijke and K.S. Sorbie, Transp. Porous Media **48**, 159 (2002).
[7] F.E. Bartell and H.J. Osterhof, Ind. Eng. Chem. **19**, 1277 (1927).
[8] R. E. Johnson and R. H. Dettre, in *Wettability*, edited by J. C. Berg Surfactant Science Series, (Dekker, New York, 1993), Vol. 49.
[9] H.L. Stone, J. Pet. Technol. **20**, 214 (1970).
[10] H.L. Stone, J. Can. Pet. Technol. **12**, 53 (1973).
[11] G.G. Pereira, W.V. Pinczewski, D.Y.C. Chan, L. Paterson, and P.E. Øren, Transp. Porous Media **24**, 167 (1996).
[12] G.G. Pereira, Phys. Rev. E **59**, 4229 (1999).
[13] V. Mani and K.K. Mohanty, SPE J. **3**, 238 (1998).
[14] D.H. Fenwick and M.J. Blunt, Adv. Water Resour. **21**, 121 (1998).
[15] C. Laroche, O. Vizika, and F. Kalaydjian, in *Proceedings of the SPE Annual Technical Conference and Exhibition* (SPE, Houston, 1999).
[16] N. R. Morrow and F. McCaffery, in *Wetting, Spreading and Adhesion*, edited by G. F. Padday (Academic Press, New York, 1978), p. 289.
[17] A.B. Dixit, S.R. McDougall, K.S. Sorbie, and J.S. Buckley, SPE Reservoir Eval. Eng. **2**, 25 (1999).
[18] D. Stauffer and X. Aharony, *Introduction to Percolation Theory*, revised 2nd ed. (Taylor and Francis, London, 1994).
[19] P.E. Øren, J. Billiote, and W.V. Pinczewski, SPE Form. Eval. **7**, 70 (1992).
[20] W.E. Soll, M.A. Celia, and J.L. Wilson, Water Resour. Res. **29**, 2963 (1993).
[21] A.A. Keller, M.J. Blunt, and P.V. Roberts, Transp. Porous Media **26**, 277 (1997).
[22] C. Laroche, in *Proceedings of the SPE European Petroleum Conference* (SPE, The Hague, 1998).
[23] M. Sohrabi, G. Henderson, D. H. Tehrani, and A. Danesh, in *Proceedings of the SPE Annual Technical Conference and Exhibition* (SPE, Dallas, 2000).
[24] M. Sohrabi, D. H. Tehrani, A. Danesh, and G. Henderson, in *Proceedings of the SPE Annual Technical Conference and Exhibition* (SPE, New Orleans, 2001).
[25] T.C. Ransohoff and C.J. Radke, J. Colloid Sci. **121**, 392 (1988).
[26] M. Dong, F.A.L. Dullien, and I. Chatzis, J. Colloid Sci. **172**, 21 (1995).
[27] J.-C. Moulu, O. Vizika, P. Egermann, and F. Kalaydjian, in *Proceedings of the SPE Annual Technical Conference and Exhibition* (SPE, Houston, 1999).
[28] M.-H. Hui and M. J. Blunt, in *Proceedings of the SPE/DOE Improved Oil Recovery Symposium* (SPE, Tulsa, 2000).
[29] M.I.J. van Dijke and K.S. Sorbie, J. Pet. Sci. Eng. **33**, 39 (2002).
[30] R. Lenormand and C. Zarcone, in *Proceedings of the International Coference on SPE/DOE Enhanced Oil Recovery Symposium* (SPE, Tulsa, 1988).

[31] P.E. Øren and W. Pinczewski, Transp. Porous Media **20**, 105 (1995).

[32] M. I. J. van Dijke, K. S. Sorbie, M. Sohrabi, D. H. Tehrani, and A. Danesh, in *Proceedings of the SPE/DOE Improved Oil Recovery Symposium* (SPE, Tulsa, 2002).

[33] T. R. Lehrdahl, P. E. Øren, and S. Bakke, in *Proceedings of the International Conference on SPE/DOE Improved Oil Recovery Symposium* (SPE, Tulsa, 2000).